Available online at www.sciencedirect.com
SCIENCE DIRECT®
Chemical Engineering and Processing xxx (2004) xxx–xxx
Chemical Engineering and Processing
www.elsevier.com/locate/cep

Kinetics of CO hydrogenation on modified Cu/ZnO catalyst in a slurry reactor

Lech Nowicki*

Faculty of Process and Environmental Engineering, Technical University of Lodz, Wolczanska 213, 90-005 Lodz, Poland

Received 15 December 2003; accepted 9 June 2004

Abstract

CO hydrogenation activity and product selectivity of a modified Cu/ZnO catalyst was investigated in a wide range of temperatures, pressures, space velocities, and synthesis gas compositions. Except alcohols, the catalyst produced a significant amount of hydrocarbons and CO_2. The formation of alcohols and hydrocarbons follows the Anderson–Schulz–Flory distribution. Based on the experimental results obtained in a stirred tank slurry reactor, a mechanistic-kinetic model was developed. The main assumption of the model was that formation of alcohols and hydrocarbons occurred independently on different types of active sites. The model successfully predicts product formation rates within the range of experimental conditions used in this study.

Keywords: Heterogeneous catalysis; Higher alcohol synthesis; Slurry reactors; Kinetic modeling; Synthesis gas

1. Introduction

In the past 25 years, there has been considerable interest in developing a process for the synthesis of higher alcohols (HAS) from CO/H_2 mixtures to be used as additives to gasoline in order to increase the octane number and reduce pollution. While methanol synthesis from syngas is practiced on a commercial scale, several higher alcohol synthesis processes are still at an experimental stage. The only exception was a 15,000 Mg/year industrial plant operated in Italy between 1982 and 1988 [1]. A modified ZnO/Cr_2O_3 catalyst was used in this technology that is known as Snamprogetti process.

Methanol and higher alcohols can be simultaneously produced from synthesis gas on many different types of catalysts. The catalysts can be classified into two categories [2]: modified Fischer–Tropsch and Group VIII metal-based catalysts, modified methanol synthesis catalysts.

The isomer distribution in the alcohol mixture involves linear primary, branched primary and linear secondary alcohols depending on the catalyst composition. Carbon monoxide is hydrogenated to primarily linear alcohols over modified Fischer–Tropsch synthesis catalysts and the alcohol product usually obeys the so-called Anderson–Schulz–Flory (ASF) distributions, i.e. the rate of alcohol formation exponentially decreases as their carbon number increases. The second class of catalysts for higher alcohols, the modified methanol synthesis catalysts, has been shown to produce a significant amount of branched alcohols and the alcohol product usually does not obey the ASF distribution.

The most studied catalysts for HAS are low-pressure methanol synthesis catalysts based on Cu and ZnO. The addition of alkali salts to binary Cu/ZnO or ternary $Cu/ZnO/Al_2O_3$ ($/Cr_2O_3$) catalyst leads to the formation of considerable amounts of higher alcohols [3–16]. Cs appears to be the most effective promoter [17], but the other alkali metals (Rb, K) can also increase the selectivity to higher alcohols [3,7]. The catalysts containing copper, alkali salt and Group VIII metal (Co, Fe, Mg) have been also reported [15,18,19]. This type of catalysts can be broadly classified as a combination of the Fischer–Tropsch and methanol catalysts.

* Tel.: +48 42 6313781; fax: +48 42 6368133.
E-mail address: nowickil@p.lodz.pl.

0255-2701/$ – see front matter © 2004 Published by Elsevier B.V.
doi:10.1016/j.cep.2004.06.002

Kinetic models for prediction of product distribution in HAS on modified Cu-based catalysts are rather scarce in the literature. Smith and Anderson [20] first modeled the kinetics of alcohol chain growth and the resulting distribution of C_{2+} alcohols based on the reaction mechanism proposed by Graves [21]. Similar approach based on a different reaction mechanism (proposed by Nunan et al. [5]) was presented by Smith et al. [22]. Breman et al. [23] developed rigorous models based on detailed reaction network and mechanism of HAS including the hydrocarbon and methyl esters formation. A lumped kinetic model for C_{2+} alcohols and separately for methanol on modified low-temperature methanol synthesis catalysts was reported by Calverley and Smith [12] and also by Kulawska and Skrzypek [16]. Syngas disappearance kinetics on Cs-doped Cu/Zn catalyst (the same as used in this study) was modeled by Nowicki and Olewski [24].

Most of the kinetic studies reported in the literature were performed in fixed bed reactors because of their simplicity. However, better and more reliable kinetic data are available from tests made in slurry stirred tank reactors because of good temperature control that enables experiments at near isothermal conditions regardless of reaction heats and rates. Small catalyst particles can be used to eliminate intraparticle mass transfer effects. Slurry stirred tank reactors have come to common use for Fischer–Tropsch and methanol synthesis studies. The first and so far the only kinetic results for the gas–slurry methanol–HAS over a Cs-Cu/ZnO/Al_2O_3 catalyst were presented by Breman et al. [25]. The presence of a slurry liquid (*n*-octacosane) appeared to affect substantially both the product distribution and the reaction mechanism relative to the gas–solid system studied earlier by the same authors (the results for corresponding gas–solid system were published in [23]).

In the present study results on the performance of the Cs-doped Cu-ZnO catalyst in a stirred tank slurry reactor in a wide range of process conditions are presented. Based on the experimental data, a new kinetic model for higher alcohol synthesis, hydrocarbon formation and the water–gas shift which can be used to describe reactant disappearance and individual product formation rates (activity and selectivity) has been developed. The model proposed in this paper can be used for the interpretation of experimental data, comparison of performance of different catalysts, and reactor modeling and simulation studies.

2. Experimental

The reactor used in this study was 1-dm^3 stainless steel autoclave of 80 mm i.d. with a magnetically driven turbine agitator (Type 1220 Haage Co., Mühlhein). The feed gases taken from cylinders (H_2 > 99.5 purity and CO > 99.3 purity) passed through a series of purification traps to remove oxygen and iron carbonyls. The feed gas flow rate and feed ratio were controlled using two calibrated mass flow controllers, and the feed was introduced into the reactor below the agitator. The stirring speed was maintained at 750 rpm, which gives the volumetric mass transfer coefficient $k_L a$ of 0.2–0.3 s^{-1} in the reaction conditions [26,27]. This was sufficient to minimize mass transfer effects between the gas and slurry phases in the reactor [28]. After leaving the reactor, the exit gas passed through a heated high-pressure separator, which condensed lower-boiling slurry liquid components. Following a backpressure regulator used to release pressure, the exit gas passed through a low-pressure ice trap to collect any condensable products. The flow rate of the tail gas exiting the system was measured using a soap film flow meter.

A kind of modified low-temperature methanol synthesis catalyst CuO/ZnO with addition of Cs, Zr, Fe, Mo, and Th oxides was synthesized by thermal decomposition of organic complexes containing metallic components of the catalyst. The catalyst samples were prepared by the Institute of Chemical Engineering, Polish Academy of Science in Gliwice, Poland.

Before testing, the catalysts was reduced with a 1/20 (by volume) H_2/He mixture passed through the reactor at the flow rate of 5.9 N m^3 kg_{cat}^{-1} h^{-1} at 453 K for 15 h. Then, the temperature was increased at the rate of 1 K/min to 493 K. This temperature was kept for 2 h with a gas mixture in which the H_2/He ratio was increased to 1/4. The activation was conducted at 0.75 MPa. The use of elevated pressure was necessary to minimize evaporation of the slurry liquid. Following the pre-treatment, the catalyst was tested at different conditions for about 200 h. The range of process conditions utilized in three runs is given in Table 1. About every 48 h, baseline conditions (593 K, 7.1 MPa, 4.5 N m^3 kg_{cat}^{-1} h^{-1}, feed gas H_2/CO = 2.3 or 583 K, 5.6 MPa, 4.5 N m^3 kg_{cat}^{-1} h^{-1}, feed gas H_2/CO = 2.3) were re-established to check deactivation properties of the catalyst.

The data at any set of process conditions were obtained during 2–5 h mass balance periods when the liquid products were allowed to accumulate in the low-pressure trap and the tail gas composition and its flow rate were measured. Tail gas samples were analyzed in two gas chromatographs: one equipped with an FID detector to quantify all oxygenates and hydrocarbons and one with a TCD detector for H_2, CO, CO_2, N_2, and CH_4. The liquid-phase product was analyzed in the GC with the FID detector.

Table 1
The experimental conditions

Catalyst: CuO/ZnO/ZrO_2/Fe_2O_3/MoO_3/ThO_2/Cs_2O
Slurry solvent: Vestowax SH-105 (Hüls AG, Germany)—the mixture of *n*-paraffins with average molecular weight of 590 g mol^{-1}
Mass of a fresh catalyst used (g): 30–40
Catalyst particle size (μm): <63 (270 mesh)
Catalyst concentration in a slurry (wt.%): 7–9
Total pressure (MPa): 4.1, 5.6, or 7.1
Temperature (K): 553, 573, 583, 593, 603, 613
Feed H_2/CO molar ratio: 0.7–2.9
Space velocity (mol kg_{cat}^{-1} s^{-1}): 0.036–0.159

3. Results and discussion

The oxygenates obtained over the catalyst used in this study contain essentially linear primary alcohols, which distribute from C_1 to C_6. Methanol is a dominant product and its concentration in the mixture is up to 60–70 wt.%. Only small amounts of branched-chain alcohols, secondary alcohols, and esters of acetic acid were also formed. Large quantities of straight-chain hydrocarbons (mainly *n*-paraffins and, to a lesser extent, 1-olefins) and CO_2 were produced in the reaction. Activity and product distributions were not affected by time-on-stream during 200 h of testing.

It is well known that Cu/ZnO catalysts modified by adding alkali salts produce C_{2+} linear alcohols with significant quantities of branched primary alcohols (mainly 2-methyl-1-propanol) [2,23]. Furthermore, a typical modified low-temperature methanol synthesis catalyst produces only a small amount of hydrocarbons and that was not the case for the catalyst used in this study. From the selectivity point of view, the catalyst is similar to the modified Fischer–Tropsch catalysts, although it contains mainly CuO and ZnO. Presumably, the addition of other metals, primarily iron (about 4 wt.% on oxide basis), has changed the catalyst properties considerably. It is interesting that similar catalyst containing the same oxides, but originating from different batch of preparation, produced very small amount of hydrocarbons under similar process conditions [16].

The effect of the addition of small amounts of iron on the performance of copper–zinc oxide methanol synthesis catalyst was investigated by Klier [29]. The idea of iron addition was to promote the chemical coupling of the C_1 methanol precursors with alkyl chains formed over an iron promoter. It was found that CO was hydrogenated to short-chain, primarily linear, alcohols and hydrocarbons. Electron microscopic investigation of the catalyst revealed that 80% of the iron dopant existed in a very fine (<10 nm) interdispersion with the copper–zinc oxide portion of the catalyst while the remaining 20% appeared as small particles of metallic iron or iron–copper cluster alloy. It is suggested that the finely interdispersed Cu/ZnO/Fe part is involved in the alcohol synthesis, while the iron metal particles are responsible for the hydrocarbon synthesis.

Experimental data obtained in this study showed that formation of both alcohols and hydrocarbons tended to follow regular trends with carbon number. The carbon number distribution of the total product (i.e. the sum of all products containing the same number of carbon atoms) is often observed in Fischer–Tropsch synthesis [30]. If chain growth occurs by the addition of the single carbon monomer unit at a time, and the rates of chain termination and propagation are independent of carbon number, then the distribution of product is given by the Schulz–Flory equation:

$$y_j = (1-\alpha)\alpha^{j-1} \tag{1}$$

where y_j indicates the mole fraction of all products containing j carbon atoms, and α is the chain growth probability, defined as the ratio of the rate of chain propagation to the total rate of chain propagation and termination ($0 \leq \alpha \leq 1$). According to this equation, the plot of $\log(y_j)$ versus j yields a straight

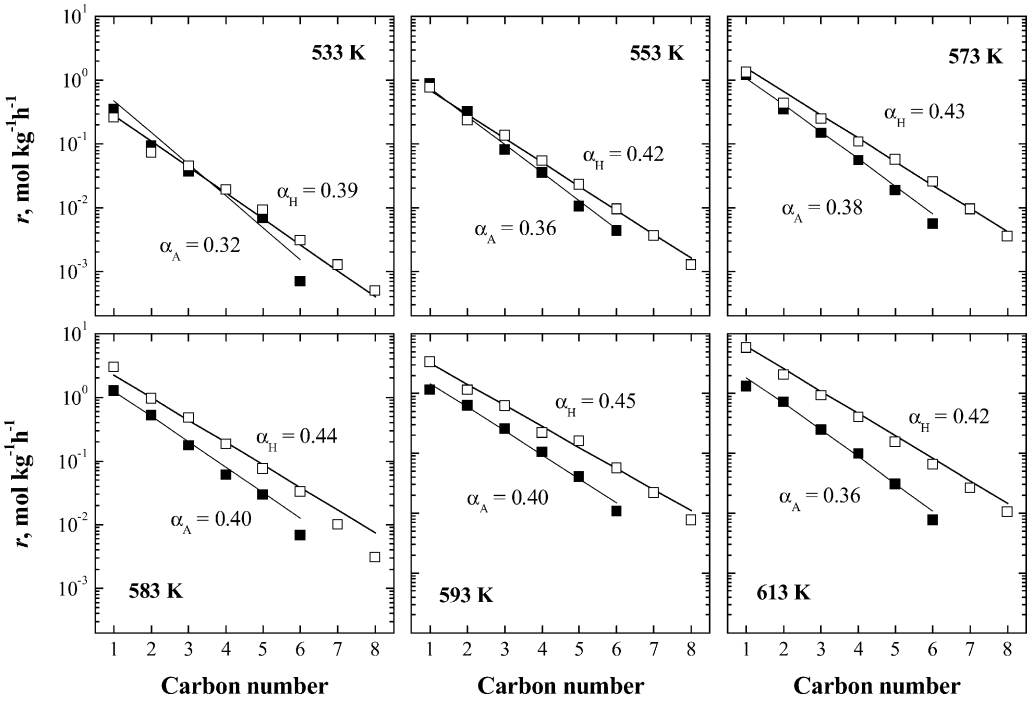

Fig. 1. Effect of temperature on product distribution in HAS (7 MPa, 0.045 mol kg^{-1} h^{-1}, H_2/CO = 2.2). Symbols are measured rates of alcohol (■) and *n*-paraffin (□) formation. Lines represent the model predictions.

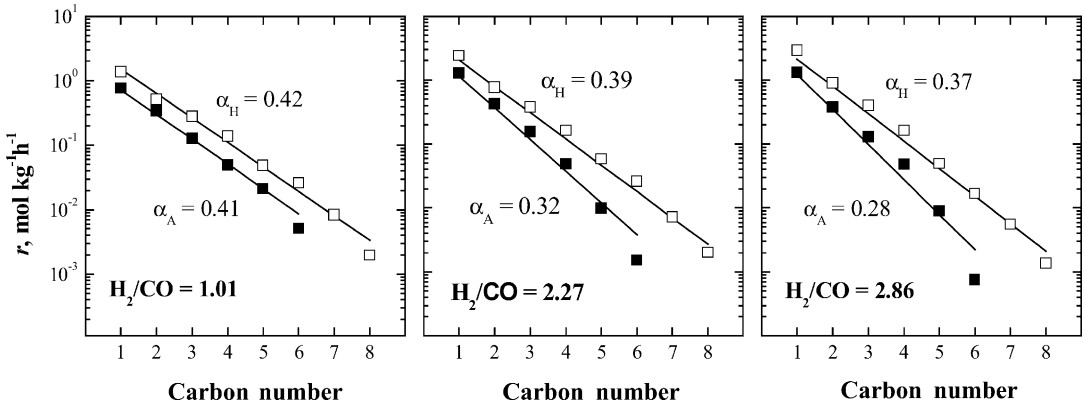

Fig. 2. Effect of syngas composition on product distribution in HAS (583 K, 5.6 MPa, 0.045 mol kg^{-1} h^{-1}). Symbols are measured rates of alcohol (■) and *n*-paraffin (□) formation. Lines represent the model predictions.

line with a slope given by log (α), and an intercept of log [(1 − α)/α)].

For individual group of products (e.g. alcohols and hydrocarbons), Eq. (1) can be used in an alternative form [31]:

$$\frac{r_j}{r_1} = \alpha^{j-1} \tag{2}$$

where r_j denotes the rate of formation of product containing j carbon atoms, and r_1 is the rate of formation of the product with one carbon atom in the molecule.

The examples of ASF distributions obtained in this study are presented in Figs. 1 and 2 (these figures will be more discussed in the next section). As can be seen from these figures, the chain growth probabilities (α_A and α_H values) for alcohols and hydrocarbons were different at the same process conditions. It may suggest that alcohols and hydrocarbons were formed by separate reaction paths. This was the main assumption made for kinetic modeling of the process described in the following section.

3.1. Modeling

A slurry stirred tank reactor was operated with a continuous flow of gas through the reactor, with batch catalyst and liquid phase. To evaluate the kinetic equation, material balances were written for the reactor with the following assumptions:

(1) The reactor is steady state and the catalyst activity is constant.
(2) The reactor is completely mixed, and temperature is uniform throughout. All heat effects are ignored. Also, the gas- and liquid-phase concentrations are uniform throughout each respective phase.
(3) The gas- and liquid-phase concentrations of all species are at their equilibrium values.
(4) Interphase and intraparticle mass transfer effects are negligible.
(5) Reaction occurs on the catalyst in the liquid phase only, and the liquid is inert.

The mass balance using these assumptions for any species j is given by a simple algebraic equation:

$$F_j^o - F_j + m_{cat} r_j = 0 \tag{3}$$

Three types of reaction are considered for higher alcohol synthesis: the formation of alcohols, the formation of *n*-paraffins, and the water–gas shift. In general, the stoichiometry of these reactions can be written as

$$nCO + 2nH_2 = C_nH_{2n+1}OH + (n-1)H_2O, \quad n = 1, \ldots, N_1 \tag{4}$$

$$nCO + (2n+1)H_2 = C_nH_{2n+2} + nH_2O, \quad n = 1, \ldots, N_2 \tag{5}$$

$$CO + H_2O = CO_2 + H_2 \tag{6}$$

The total number of species considered, S, is given by (N_1 + N_2 + 3), where N_1 and N_2 are the maximum carbon number products for alcohols and hydrocarbons, respectively. Thus, Eq. (3) can be written for all alcohols, hydrocarbons, and CO_2, whereas the molar flow rates of CO, H_2, and H_2O are calculated most easily by stoichiometry balance equations:

$$F_{CO} = F_{CO}^o - \sum_{n=1}^{N_1} n F_{A,n} - \sum_{n=1}^{N_2} n F_{H,n} - F_{CO_2} \tag{7}$$

$$F_{H_2} = F_{H_2}^o - \sum_{n=1}^{N_1} 2n F_{A,n} - \sum_{n=1}^{N_2} (2n+1) F_{H,n} + F_{CO_2} \tag{8}$$

$$F_{H_2O} = F_{H_2O}^o - \sum_{n=1}^{N_1} (n-1) F_{A,n} - \sum_{n=1}^{N_2} n F_{H,n} - F_{CO_2} \tag{9}$$

The total species reaction rates, r_j, are given by the kinetic model described below. Solving balance equations (Eqs. (3) and (7)–(9)) for known kinetic expressions gives the outlet molar flow rates of individual components, which can be used to calculate their partial pressures. In fact, reaction rates

are the functions of temperature and liquid-phase concentrations in a slurry reactor; however, it is more convenient to use gas-phase partial pressures in place of liquid concentrations. Under assumption (3) above, the gas- and liquid-phase concentrations of gaseous species are in equilibrium. Under these circumstances, the partial pressures and liquid concentrations can be related directly by $c_j = \mathrm{He}_j P_j$. The use of liquid concentrations, activities, or partial pressures will affect the dimensions of any constants in the rate expressions. Furthermore, since Henry's law constants are the functions of temperature, activation energies will also change when different concentration terms are used. The Henry's law constants for synthesis gas components, carbon dioxide, and water have been well studied over a wide range of temperature (75–300 °C) in pure Vestowax by Nettelhoff et al. [32].

The kinetic model for higher alcohol synthesis product formation presented in this paper was developed using Langmuir–Hinselwood–Hougen–Watson approach, which included formation of normal alcohols and normal paraffins. The model was derived under the following assumptions:

(1) There are two types of active sites on the catalyst surface: type-1, where growth of alcohol intermediates occurs, and type-2, where hydrocarbon precursors are formed.
(2) The formation of alcohols and hydrocarbons occurs via different intermediates.
(3) There is no net accumulation of reactants or products on the surface of the catalyst.
(4) No mass transfer limitations exist between the surface of the catalyst and the bulk gas phase.
(5) Only hydrogen, CO, and monomers $CH_2O\#1$ or $CH_2\#2$ occupy a significant fraction of the catalyst sites.
(6) Termination reactions leading to alcohols and hydrocarbons are rate-determining steps.

A detailed reaction network for linear alcohols from syngas is based on CO insertion mechanism. The carbide mechanism by methylene monomer (CH_2) insertion into adsorbed alkyl groups was considered for the chain growth in the hy-

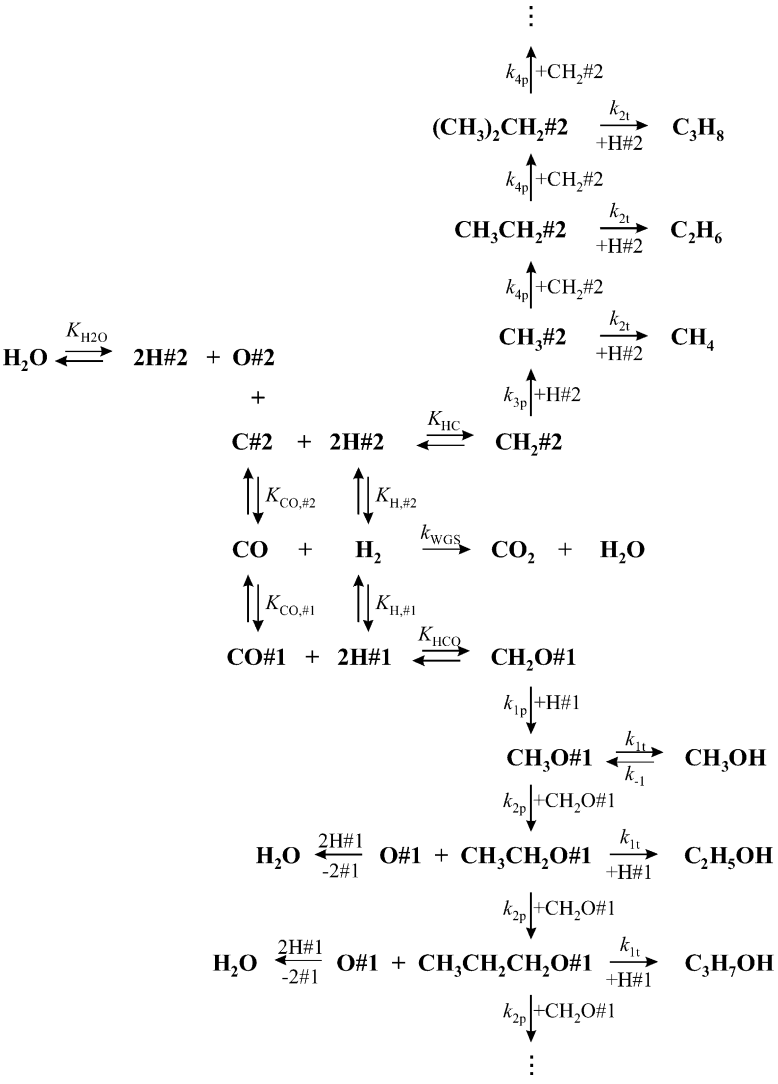

Fig. 3. The network of elementary steps in higher alcohol synthesis system.

drocarbon formation during higher alcohol synthesis. Elementary steps in the synthesis of *n*-alcohols, *n*-paraffins, and water–gas-shift reaction are proposed in Fig. 3.

According to assumed mechanisms, CO adsorbs directly on active sites #1 or dissociatively on active sites #2, while H_2 adsorbs dissociatively on both types of the sites. The surface concentrations of inorganics can be obtained by assuming equilibrium adsorption for CO and H_2. Steady-state mass balances (using pseudo-steady-state approximation) for surface intermediates adsorbed on active sites #1 and #2 can be written to account for their surface concentrations. For example, for any alkyl species adsorbed on active sites #2 containing *n* carbon atoms, the rate of propagation of the $(n-1)^{\text{th}}$ species must equal the combined rates of propagation and termination of the n^{th} species. The steady-state balance for the hydrocarbon surface species is then

$$k_{4p}[R_{n-1}\#2][\text{H}\#2] = k_{4p}[\text{CH}_2\#2][R_n\#2] + k_{2t}[\text{H}\#2][R_n\#2] \tag{10}$$

where, for convenience, the $(CH_2)_nH$ species has been denoted as R_n. This equation is valid for all $n \geq 2$, and solving it for $[R_n\#2]$ yields

$$[R_n\#2] = \frac{k_{4p}[R_{n-1}\#2][\text{H}\#2]}{k_{4p}[\text{CH}_2\#2] + k_{2t}[\text{H}\#2]} \tag{11}$$

Summary of the higher alcohol synthesis kinetic model equations is given in Table 2. To reduce a number of kinetic parameters, simple mass action kinetics was assumed for the water–gas shift reaction.

By its definition, the Schulz–Flory chain growth probability for alcohols, α_A, is the rate of chain propagation divided by the sum of the rates of chain propagation and termination. In terms of the rate equations obtained, α_A is then given by

$$\alpha_A = \frac{k_{2p}[\text{CH}_2\text{O}\#1]}{k_{2p}[\text{CH}_2\text{O}\#1] + k_{1t}[H\#1]} \tag{12}$$

The combination of Eq. (12) with the expressions for surface concentrations of the monomer and hydrogen atom given in Table 2 leads to the following formula:

$$\alpha_A = \frac{1}{1 + (k_{1t}/k_{2p})(\eta_2/\eta_1)(1/p_{CO}p_{H_2}^{1/2})} \tag{13}$$

and similarly for hydrocarbons:

$$\alpha_H = \frac{1}{1 + (k_{2t}/k_{4p})(\eta_4/\eta_3)(1/(p_{CO}p_{H_2})^{1/2})} \tag{14}$$

The 14 parameters appearing in the kinetic model (k_{1p}, k_{2p}, k_{3p}, k_{4p}, k_{1t}, k_{2t}, k_{-1}, $K_{CO,\#1}$, η_1,..., η_5, k_{WGS}) were estimated by minimizing the residual sum of squares for all alcohols, hydrocarbons, and CO_2 at different temperatures.

Table 2
Kinetic model equations of the higher alcohol synthesis

$$r_{A,1} = k_{1t}[\text{CH}_3\text{O}\#1][\text{H}\#1] - \frac{k_{-1}p_{\text{CH}_3\text{OH}}}{ad_1^2}$$

$$r_{A,n} = k_{1t}[R_n\text{O}\#1][\text{H}\#1], \quad n = 2, 3, ..., N_1$$

where

$$[\text{CH}_3\text{O}\#1] = \frac{k_{1p}[\text{CH}_2\text{O}\#1][\text{H}\#1] + k_{-1}p_{\text{CH}_3\text{OH}}/ad_1^2}{k_{2p}[\text{CH}_2\text{O}\#1] + k_{1t}[\text{H}\#1]}$$

$$[R_n\text{O}\#1] = \frac{k_{2p}[R_{n-1}\text{O}\#1][\text{CH}_2\text{O}\#1]}{k_{2p}[\text{CH}_2\text{O}\#1] + k_{1t}[\text{H}\#1]}, \quad n = 2, 3, \ldots, N_2$$

$$[\text{CH}_2\text{O}\#1] = \frac{\eta_1 p_{CO}p_{H_2}}{ad_1} \qquad [\text{H}\#1] = \frac{\eta_2 p_{H_2}^{1/2}}{ad_1}$$

$$ad_1 = 1 + \eta_1 p_{CO}pH_2 + \eta_2 p_{H_2}^{1/2} + K_{CO,\#1}p_{CO}$$

$$\eta_1 = K_{HCO}K_{CO,\#1}K_{H,\#1} \qquad \eta_2 = (K_{H,\#1})^{1/2}$$

$$r_{H,n} = k_{2t}[R_n\#2][\text{H}\#2], \quad n = 1, 2, ..., N_2$$

where

$$[R_1\#2] = \frac{k_{3p}[\text{CH}_2\#2][\text{H}\#2]}{k_{4p}[\text{CH}_2\#2] + k_{2t}[\text{H}\#2]}$$

$$[R_n\#2] = \frac{k_{4p}[R_{n-1}\#2][H\#2]}{k_{4p}[CH_2\#2] + k_{2t}[H\#2]}, \quad n = 2, 3, \ldots, N_2$$

$$[\text{CH}_2\#2] = \frac{\eta_3 p_{CO}^{1/2}p_{H_2}}{ad_2} \qquad [\text{H}\#2] = \frac{\eta_4 p_{H_2}^{1/2}}{ad_2}$$

$$ad_2 = 1 + \eta_3 p_{CO}^{1/2}p_{H_2} + \eta_4 p_{H_2}^{1/2} + \eta_5 p_{CO}^{1/2}$$

$$\eta_3 = K_{HCO}K_{CO,\#2}^{1/2}K_{H,\#3}, \qquad \eta_4 = (K_{H,\#2})^{1/2}, \qquad \eta_5 = (K_{CO,\#2})^{1/2}$$

$$r_{WGS} = k_{WGS}\left(p_{CO}p_{H_2O} - \frac{p_{CO_2}p_{H_2}}{K_{p,WGS}^*}\right)$$

$$\ln K_{p,WGS}^* = \frac{4577.8}{T} - 4.33 \text{ [33]}$$

$$J = \frac{1}{M}\sum_{i=1}^{M}\left[\sum_{n=1}^{N_1}\left|\frac{r_{A,n}^{calc} - r_{A,n}^{exp}}{r_{A,n}^{exp}}\right| + \sum_{n=1}^{N_2}\left|\frac{r_{H,n}^{calc} - r_{H,n}^{exp}}{r_{H,n}^{exp}}\right| + \left|\frac{r_{CO_2,n}^{calc} - r_{CO_2,n}^{exp}}{r_{CO_2,n}^{exp}}\right|\right] \tag{15}$$

where *M* is the total number of experiments made at different pressures, space velocity and feed H_2/CO ratio. The calculations were performed for six alcohols and eight hydrocarbons. Depending on temperature, *M* was between 6 and 14. By taking $N_1 = 6$ and $N_2 = 8$, the set of 15 nonlinear algebraic Eq. (1) was solved by Newton–Raphson method for each experiment. Six sets of kinetic parameters were obtained for six different temperatures. To establish the kinetic parameters as a function of temperature, the following equation was used:

$$k_i = A_i \exp\left(-\frac{B_i}{RT}\right) \tag{16}$$

where k_i denotes a model parameter, A_i is the pre-exponential factor, and B_i is the activation energy for a rate constant or heat of adsorption for adsorption equilibrium constant and

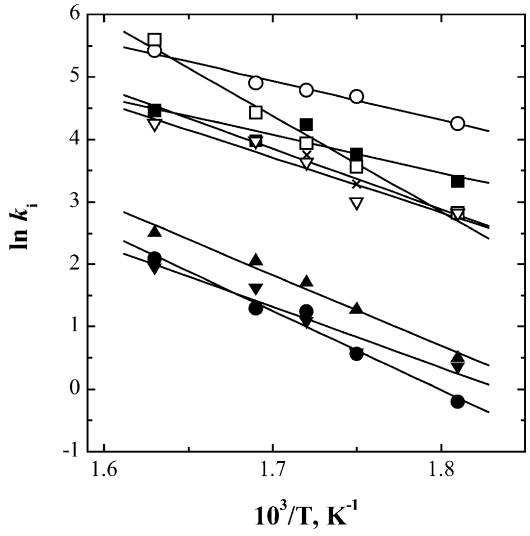

Fig. 4. Arrhenius plot for reaction rate constants: k_{1p} (■),k_{2p} (●),k_{3p} (□),k_{4p} (×),k_{1t} (▲),k_{2t} (▽), k_{-1} (▼),k_{WGS} (◯).

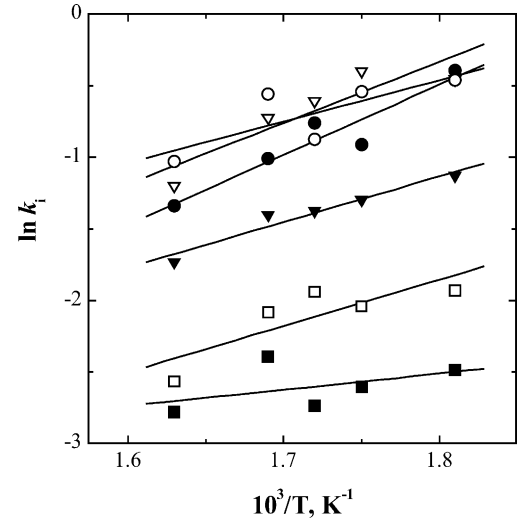

Fig. 5. van't Hoff plot for adsorption equilibrium constants: η_1 (■),η_2 (▼),η_3 (□),η_4 (▽),η_5 (◯), K_{CO} (●).

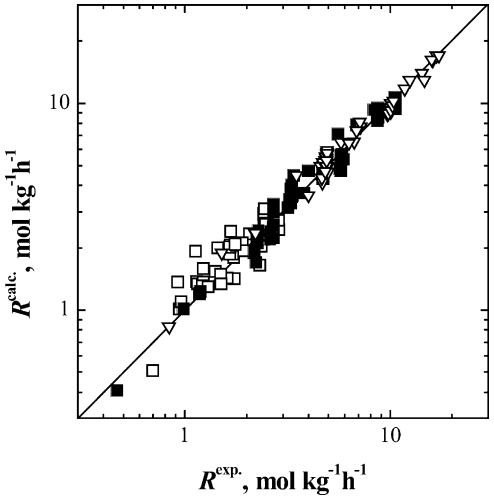

Fig. 6. Parity plot of higher alcohol synthesis (▽: CO_2, □: *n*-alcohol, ■: *n*-paraffin).

then $B_i < 0$. The Arrhenius plots for the rate constants are presented in Fig. 4, whereas the van't Hoff relationships for equilibrium constant group are shown in Fig. 5. The good linearity confirms the validity of Eq. (16). The values of parameters *A* and *B* found from linear regression of the data shown in Figs. 4 and 5 are listed in Table 3.

The parity plot for lumped rate of alcohol formation, lumped rate of hydrocarbon formation and CO_2 formation is given in Fig. 6. To calculate these rates, the parameter values from Table 3 were used. The agreement is good as the deviations are random and do not show any trends.

The comparison between observed and predicted formation rates for alcohols and hydrocarbons can be better seen from Figs. 1 and 2. Symbols represent the experimental results and lines model predictions. The chain probability factors α_A for alcohols and α_H for hydrocarbons obtained based on calculated rates of formations are also given in the figures.

In Fig. 1, the data for all reaction temperatures covered in this study and one selected pressure, space velocity, and feed gas composition are shown. An increase in tempera-

Table 3
The values of kinetic parameters

Parameter	*A*	*B* (kJ mol^{-1})	Correlation coefficient
k_{1p}	2.03×10^6 kg$_{cat}$ mol^{-1} h^{-1}	51.2	0.93
k_{2p}	1.14×10^{10} kg$_{cat}$ mol^{-1} h^{-1}	107	0.99
k_{1t}	$2.86 \cdot \times 10^9$ kg$_{cat}$ mol^{-1} h^{-1}	96.1	0.99
k_{-1}	6.82×10^7 mol kg$_{cat}^{-1}$ MPa^{-1} h^{-1}	81.9	0.96
η_1	1.05×10^{-2} MPa^{-2}	−9.44	0.46
η_2	9.74×10^{-4} MPa$^{-1/2}$	−26.9	0.96
$K_{CO,\#1}$	7.77×10^{-2} MPa^{-1}	−41.5	0.95
k_{3p}	2.08×10^{13} kg$_{cat}$ mol^{-1} h^{-1}	129	0.81
k_{4p}	8.71×10^8 kg$_{cat}$ mol^{-1} h^{-1}	82.0	0.99
k_{2t}	1.54×10^8 kg$_{cat}$ mol^{-1} h^{-1}	74.1	0.96
η_3	4.70×10^{-4} MPa$^{-3/2}$	−26.80	0.81
η_4	3.28×10^{-4} MPa$^{-1/2}$	−35.6	0.88
η_5	3.37×10^{-3} MPa$^{-1/2}$	−24.2	0.78
k_{WGS}	6.10×10^6 mol kg$_{cat}^{-1}$ MPa^{-2}h^{-1}	52.4	0.99

ture results in higher hydrocarbon selectivity. At the lowest temperature (533 K), the rates of formation of hydrocarbons and alcohols are comparable, whereas at higher temperatures, hydrocarbons are produced faster than alcohols, so their concentrations in the reactor outlet are also higher. As it was mentioned before, the alcohol products and the hydrocarbons obey separate ASF distributions with different temperature-dependent coefficients for the chain growth probabilities. The chain growth probability and thus the selectivity must change with temperature as all kinetic parameters appearing in Eqs. (13) and (14) are temperature dependent. In the range of 533–593 K, both α_A and α_H increase when temperature increases, and it means that the product selectivity shifts toward heavier products. However, at 613 K, the chain growth probabilities become smaller because of significant decrease of partial pressures of syngas components caused by high conversion at this temperature.

The expected effect of partial pressures and total pressure individually on the chain growth probability can be seen directly from Eqs. (13) and (14). As the total pressure increases, both p_{CO} and p_{H_2} will increase, and α will approach unity as the right terms in the denominator of Eq. (13) or (14) become small. The results show that product selectivity shifts to heavier products and to more alcohols and hydrocarbons with increasing total pressure.

Increasing H_2/CO ratios in the feed gas results in higher alcohol and hydrocarbon productivity and in more lighter alcohols in the alcohol product mixture. The chain growth probability α_A decreased from 0.41 to 0.28 by increasing the H_2/CO ratio from 1.01 to 2.86 (see Fig. 2). At the same time, the α_H value decreased from 0.42 to 0.37; thus, the feed gas composition has lower impact on hydrocarbon selectivity.

Appendix A. Nomenclature

List of symbols

A, B	formal parameters of the model
c	concentration (mol m^{-3})
F	molar flow rate (mol h^{-1})
He	Henry's constant (mol m^{-3} MPa^{-1})
J	sum of absolute relative residuals
K	chemical equilibrium constant
k	reaction rate constant
m_{cat}	mass of catalyst (kg)
n	number of carbon atoms
p	partial pressure (MPa)
R	gas constant (8.314 J mol^{-1} K^{-1})
r	rate of formation (mol kg$_{cat}^{-1}$ h^{-1})
T	temperature (K)
y	mole fraction
α	chain growth probability
η	model parameter

Subscripts

n	carbon number
A	alcohol
H	hydrocarbon (*n*-paraffin)

Superscripts

o	inlet

References

[1] A. Paggini, D. Sanfilippo, G. Pecci, I. Dybkjaer, Implementation of the methanol plus higher alcohols process by Snamprogetti Enichem, Haldor Topsoe A/S MAS Technology, in: Proceedings of the Seventh Int. Symp. Carbur. Alohols, 1986, pp. 62–67.
[2] P. Forzatti, E. Tronconi, P. Italo, Higher alcohol synthesis, Catal. Rev. -Sci. Eng. 33 (1, 2) (1991) 109–168.
[3] K.J. Smith, R.B. Anderson, The higher alcohol synthesis over promoted copper/zinc oxide catalyst, Can. J. Chem. Eng. 61 (1983) 40–45.
[4] M. Calverley, R.B. Anderson, Synthesis of higher alcohols over promoted copper catalysts, J. Catal. 104 (1987) 434–440.
[5] J.G. Nunan, C.E. Bogdan, K. Klier, K.J. Smith, C.-W. Young, R.G. Herman, Methanol and C_2 oxygenate synthesis over cesium doped Cu/ZnO and Cu/ZnO/Al_2O_3 catalysts. A study of selectivity and ^{13}C incorporation patterns, J. Catal. 113 (1988) 410–433.
[6] D.J. Elliot, F. Pannella, Mechanisms of ethanol formation from synthesis gas over CuO/ZnO/Al_2O_3, J. Catal. 114 (1988) 90–99.
[7] J.G. Nunan, C.E. Bogdan, K. Klier, K.J. Smith, C.-W. Young, R.G. Herman, Higher alcohol and oxygenate synthesis over cesium-doped Cu/ZnO catalysts, J. Catal. 116 (1989) 195–221.
[8] J.G. Nunan, R.G. Herman, K. Klier, Higher alcohol synthesis over Cs/ZnO/M_2O_4 (M=Al, Cr) catalysts, J. Catal. 116 (1989) 222–229.
[9] D.J. Elliot, F. Pannella, The formation of ketones in the presence of carbon monoxide over CuO/ZnO/Al_2O_3, J. Catal. 118 (1988) 359–367.
[10] A.B. Stiles, F. Chen, J.B. Harrison, X. Hu, D.A. Storm, H.X. Yang, Catalytic conversion of synthesis gas to methanol and other oxygenated products, Ind. Eng. Chem. Res. 30 (1991) 811–821.
[11] A. Kiennemann, H. Idriss, R. Kieffer, P. Chaumette, D. Durand, Study of the mechanism of higher alcohol synthesis on Cu-ZnO-Al_2O_3 catalysts by catalytic tests, probe molecules, ad temperature programmed desorption studies, Ind. Eng. Chem. Res. 30 (1991) 1130–1138.
[12] E.M. Calverley, K.J. Smith, Kinetic model for alcohol synthesis over a promoted Cu/ZnO/Cr_2O_3 catalyst, Ind. Eng. Chem. Res. 31 (1992) 792–803.
[13] J.C. Slaa, J.G. van Ommen, J.R.H. Ross, The synthesis of hugher alcohols using modified Cu/ZnO/Al_2O_3 catalysts, Catal. Today 15 (1992) 129–148.
[14] J.M. Campos-Martin, A. Guerrero-Ruiz, J.L.G. Fierro, Structural and surface properties of CuO-ZnO-Cr_2O_3 catalysts and their relationship with selectivity to higher alcohol synthesis, J. Catal. 156 (1995) 208–218.
[15] A.-M. Hilmen, M. Xu, M.J.L. Gines, E. Iglesia, Synthesis of higher alcohols on copper catalysts supported on alkali-promoted basic oxides, Appl. Catal. A 169 (1988) 355–372.
[16] M. Kulawska, J. Skrzypek, Kinetics of the synthesis of higher aliphatic alcohols from syngas over a modified methanol synthesis catalyst, Chem. Eng. Proc. 30 (2001) 33–40.
[17] G.A. Vedage, P.B. Himelfarb, G.W. Simmons, K. Klier, Alkali-promoted copper–zinc oxide catalysts for low alcohol synthesis, in: Solid State Chemistry in CatalysisACS Symp. Ser., 279, 1985, p. 295.

[18] K. Klier, Catalytic chemistry of low alcohol synthesis—following E.B. Anderson lead, in: S. Kaliaguine, A. Mahay (Eds.), Catalysis on the Energy Scene, Elsevier, Amsterdam, 1984, pp. 439–455.
[19] C.R. Apesteguia, B. De Rites, S. Miseo, S. Soled, Catalysts for producing methanol and isobutanol mixtures from synthesis gas, Catal. Lett. 44 (1997) 1–5.
[20] K.J. Smith, R.B. Anderson, A chain growth scheme for the higher alcohols synthesis, J. Catal. 85 (1984) 428–436.
[21] G.D. Graves, Higher alcohols formed from carbon monoxide and hydrogen, Ind. Eng. Chem. 23 (1931) 1381–1385.
[22] K.J. Smith, C.W. Young, R.G. Herman, K. Klier, Development of a kinetic model for alcohol synthesis over a cesium-promoted Cu/ZnO catalyst, Ind. Eng. Chem. Res. 30 (1991) 61–71.
[23] B.B. Breman, A.C.C.M. Beenackers, E. Oesterholt, A kinetic model for the methanol-higher alcohol synthesis from $CO/CO_2/H_2$ over Cu/ZnO-based catalysts including simultaneous formation of methyl esterd and hydrocarbons, Chem. Eng. Sci. 49 (24A) (1994) 4409–4428.
[24] L. Nowicki, T. Olewski, Kinetics of the overall higher alcohol synthesis reacting system, Chem. Paper 57 (1) (2003) 21–25.
[25] B.B. Breman, A.C.C.M. Beenackers, H.A. Schuurman, E. Oesterholt, Kinetics of the gas-slurry methanol-higher alcohol synthesis from $CO/CO_2/H_2$ over a Cs-Cu/ZnO/Al_2O_3 catalyst including simultaneous formation of methyl esters and hydrocarbons, Catal. Today 24 (1995) 5–14.
[26] S. Ledakowicz, H. Nettelhoff, W.-D. Deckwer, Gas–liquid mass transfer data in a stirred autoclave reactor, Ind. Eng. Chem. Fundam. 23 (1984) 510–512.
[27] S. Ledakowicz, L. Nowicki, M. Stelmachowski, W. Kotowski, Absorption of synthesis gas components under conditions of methanol synthesis in liquid phase, Inz. Chem. Procesowa 2 (1988) 281–291.
[28] G.H. Graf, J.G.M. Winkelman, E.J. Stamhuis, A.A.C.M. Beenackers, Kinetics of the three phase methanol synthesis, Chem. Eng. Sci. 43 (1988) 2161–2168.
[29] K. Klier, Catalytic chemistry of low alcohol synthesis—following E.B. Anderson lead., in: S. Kaliaguine, A. Mahay (Eds.), Catalysis on the Energy Scene, Elsevier, Amsterdam, 1984, pp. 439–455.
[30] R.B. Anderson, The Fischer–Tropsch Synthesis, Academic Press, New York, 1984.
[31] H. Schulz, M. Claeys, Kinetic modeling of Fischer–Tropsch product distributions, Appl. Catal. A: Gen. 186 (1999) 91–107.
[32] H. Nettelhoff, R. Kokuun, S. Ledakowicz, W.-D. Deckwer, Studies on the kinetics of Fischer–Tropsch synthesis in slurry phase, Ger. Chem. Eng. 8 (1985) 177–181.
[33] D.S.C. Newsome, The water–gas shift reaction, Catal. Rev. -Sci. Eng. 21 (1980) 275–318.